

Microscopic magnetic and structural nature of spinel $\text{Li}[\text{Li}_x\text{Mn}_{2-x}]\text{O}_4$

J. Sugiyama,^{1,*} K. Mukai,¹ Y. Ikedo,¹ P. L. Russo,² T. Suzuki,³ I. Watanabe,³ J. H. Brewer,⁴ E. J. Ansaldo,² K. H. Chow,⁵ K. Ariyoshi,⁶ and T. Ohzuku⁶

¹Toyota Central Research and Development Laboratories Inc., Nagakute, Aichi 480-1192, Japan

²TRIUMF, 4004 Wesbrook Mall, Vancouver, British Columbia, Canada V6T 2A3

³Muon Science Laboratory, RIKEN, 2-1 Hirosawa, Wako, Saitama 351-0198, Japan

⁴TRIUMF, CIAR, and Department of Physics and Astronomy, University of British Columbia, Vancouver, British Columbia, Canada V6T 1Z1

⁵Department of Physics, University of Alberta, Edmonton, Alberta, Canada T6G 2G7

⁶Department of Applied Chemistry, Graduate School of Engineering, Osaka City University, Osaka 558-8585, Japan

(Received 2 April 2007; published 17 May 2007)

The magnetic nature of the spinel antiferromagnet $\text{Li}[\text{Li}_x\text{Mn}_{2-x}]\text{O}_4$ with $x=0-0.15$ has been studied with muon-spin rotation and relaxation ($\mu^+\text{SR}$) spectroscopy. Both weak-transverse-field and zero-field $\mu^+\text{SR}$ measurements indicate that the whole sample enters into a static disordered magnetic phase below T_N for all the samples measured; $T_N=61$ K for LiMn_2O_4 , but 27–23 K for the $x=0.05-0.15$ samples. It was also clarified that both the field distribution width and the field fluctuation rate show a clear change at the Jahn-Teller (JT) transition temperature ($T_{\text{JT}}=280$ K) for LiMn_2O_4 , and a short-range cooperative JT distortion appears below 280 K even for $\text{Li}[\text{Li}_{0.15}\text{Mn}_{1.85}]\text{O}_4$.

DOI: 10.1103/PhysRevB.75.174424

PACS number(s): 75.25.+z, 64.70.Kb, 75.50.Ee, 76.75.+i

I. INTRODUCTION

In the cubic $(A)_{8a}[B_2]_{16d}\text{O}_4$ spinel lattice with space group $Fd\bar{3}m$ (see Fig. 1), where A ions are located in the tetrahedral $8a$ sites and B ions in the octahedral $16d$ sites, four B ions form a tetrahedron, indicating the existence of three-dimensional geometrical frustration for magnetic B ions with an antiferromagnetic (AF) interaction. For the $(\text{Li})_{8a}[\text{Li}_x\text{Mn}_{2-x}]_{16d}\text{O}_4$ (LMO) spinels, which are heavily investigated as a positive electrode material for rechargeable lithium batteries,¹ magnetic Mn^{3+} ions with $S=2$ ($t_{2g}^3e_g^1$) and Mn^{4+} ions with $S=3/2$ (t_{2g}^3) sit only at the $16d$ site, while the $8a$ sites are occupied by nonmagnetic Li^+ ions. The excess Li^+ ions located at the $16d$ site not only dilute the magnetic interaction but also increase the average valence of the Mn ions (V_{Mn}). That is, $V_{\text{Mn}}=3.5$ for LiMn_2O_4 , and as x increases from 0, V_{Mn} increases in proportion to x , and reaches 4 for $\text{Li}[\text{Li}_{1/3}\text{Mn}_{5/3}]\text{O}_4$.

The stoichiometric compound (LMO with $x=0$) exhibits two phase transitions; one is a structural transition from a high- T cubic phase to a low- T orthorhombic phase at $T_{\text{JT}} \sim 280$ K induced by a cooperative Jahn-Teller (JT) distortion of Mn^{3+} ions,²⁻⁴ and the other is an AF transition with $T_N \sim 60$ K, which was found by ^7Li -NMR,⁵ and then confirmed by neutron diffraction experiments.⁶⁻⁸ Since both neutron and electron diffraction analyses indicated charge ordering of Mn^{3+} and Mn^{4+} below T_{JT} that is probably stabilized by the cooperative JT distortion,⁹ the AF order is also considered to be strongly coupled with charge ordering.

For LMO with $x>0$, T_{JT} was reported to decrease with increasing x down to 214 K at $x=0.035$ and then to disappear with further increasing x by a differential scanning calorimetry (DSC) analysis, due to the decrease in the amount of JT-active Mn^{3+} ions,¹⁰ while the recent elastic-anelastic measurements on LMO with $0 \leq x \leq 0.08$ indicated the existence of the JT transition even for the $x=0.08$ sample (T_{JT}

~ 210 K).¹¹ On the other hand, neutron diffraction measurements indicated that the Mn^{3+} ions in LMO with $x=0.04$ are in a low-spin state (t_{2g}^4), meaning the absence of the JT distortion or transition.¹² Moreover, since the Li^+ ions at the $16d$ site cause deviation of the ratio of Mn^{3+} to Mn^{4+} from 1, charge ordering is expected to be hindered because of mismatch in the period between lattice and charge order. Actually, LMO with $x=0.04$ lacks charge ordering down to 4 K, although $\text{Li}[\text{Li}_{0.04}\text{Mn}_{1.96}]\text{O}_4$ exhibited a spin-glass-like transition at $T_f \sim 25$ K.¹² For LMO with $x \geq 0.1$, T_f is reported to decrease from 23 K for $x=0.1$ to 10 K for $x=0.33$ by susceptibility measurements.¹³

Coherent precession of muon spins signals the appearance of magnetically ordered states even if the order is not long range, provided it is (quasi) static on the microsecond time scale. A positive muon-spin rotation and relaxation ($\mu^+\text{SR}$) technique is thus very suitable for detecting short-range magnetic order, which often appears in frustrated systems. Past

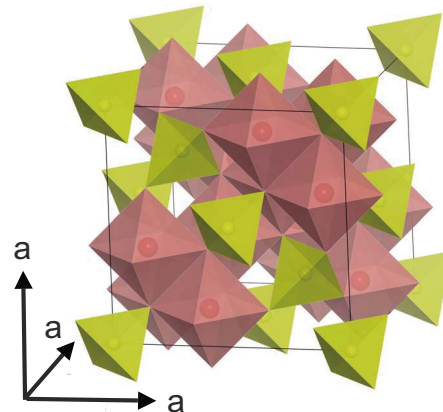


FIG. 1. (Color online) Crystal structure of cubic LiMn_2O_4 spinel. Li ions locate at the $8a$ site (center of the LiO_4 tetrahedron), while Mn ions at the $16d$ site (center of the MnO_6 octahedron).

μ^+ SR experiments on powder LMO samples were, however, mainly concentrated on the μ^+ diffusion behavior above 100 K, to study the relationship between μ^+ and Li⁺ diffusion.^{14,15}

In order to elucidate the change in magnetism of LMO by x , we measured μ^+ SR spectra down to 1.8 K using powder samples of LMO with $x=0, 0.05, 0.1$, and 0.15 . We clearly demonstrated that all samples exhibited a magnetic transition below 61 K (T_N or T_f), and, moreover, the whole sample enters into the magnetic phase below T_N or T_f . Furthermore, the detailed analysis of zero-field (ZF) and longitudinal-field (LF)- μ^+ SR spectra shows that a short-range cooperative JT distortion still exists even in LMO with $x=0.15$, and the onset of the transition temperature ($T_{\text{SRJT}}^{\text{on}} \sim 280$ K) is almost independent of x and the same as T_{JT} . This result suggests that μ^+ SR is the only technique that is able to provide crucial information on $T_{\text{SRJT}}^{\text{on}}$ in these technologically relevant systems.

II. EXPERIMENT

Powder samples of LMO with $x=0, 0.05, 0.1$, and 0.15 were prepared at OCU from $\text{LiOH}\cdot\text{H}_2\text{O}$ and MnOOH . The mixture was pressed into a pellet of 23 mm diameter and ~ 5 mm thickness, and heated at 1000 °C for 12 h in air to develop crystallites. The obtained powder was crushed, repressed into a pellet, and then oxidized at 700, 650, 600, and 575 °C for 24 h in air for LMO with $x=0, 0.05, 0.1$, and 0.15 , respectively.

The particle morphology of all the samples was an octahedral shape with smooth (111) facets. Powder x-ray diffraction (XRD) studies indicated that the four samples were single phase of a cubic structure with space group $Fd\bar{3}m$. The lattice parameters of the $x=0, 0.05, 0.1$, and 0.15 samples were calculated as $a=0.8240(5), 0.8223(7), 0.8207(3)$, and $0.8193(4)$ nm, respectively. According to an inductively coupled plasma-atomic emission spectrometry analysis, the Li to Mn ratios of the four samples were 1.00:2.00, 1.04:1.96, 1.09:1.91, and 1.15:1.85, respectively. The samples were then examined by an electrochemical charge-discharge test using a $\text{Li}|\text{LiPF}_6\text{-ethylene carbonate-dimethyl carbonate}|\text{Li}[\text{Li}_x\text{Mn}_{2-x}]\text{O}_4$ cell. All the samples showed electrochemical reactivity in the nonaqueous lithium cell.¹⁶ We restrict our studies to LMO with $x \leq 0.15$ because of Li_2MnO_3 contamination when $x \geq 0.2$.¹⁶

The susceptibility (χ) was measured using a superconducting quantum interference device magnetometer (MPMS, Quantum Design) in the T range between 5 and 400 K under magnetic field $H \leq 55$ kOe. For the μ^+ SR experiments, the powder was pressed into a disk of about 20 mm diameter and 1 mm thickness, and subsequently placed on a silver sample holder or in a muon-veto sample holder. The μ^+ SR spectra were measured in the surface muon beam line at the ARGUS surface muon beam line of the RIKEN-RAL Muon Facility at the ISIS and the M20 surface muon beam line at TRIUMF. The experimental setup and techniques are described in more detail elsewhere.¹⁷

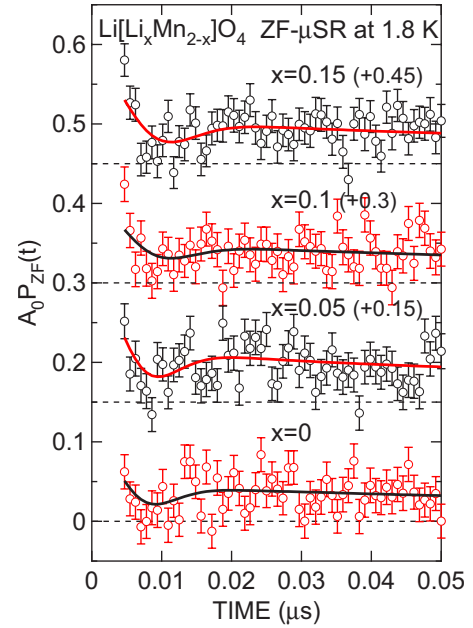


FIG. 2. (Color online) ZF- μ^+ SR spectrum for LMO with $x=0, 0.05, 0.1$, and 0.15 at 1.8 K obtained at TRIUMF. Each spectrum is offset by 0.15 for clarity of the display. The first minimum around $0.01 \mu\text{s}$ is a characteristic feature of a Kubo-Toyabe-type relaxation, indicating the existence of randomly oriented magnetic moments.

III. RESULTS AND DISCUSSION

A. Magnetic transition below ~ 60 K

We have measured ZF- μ^+ SR spectra in LiMn_2O_4 below 320 K to know the change in magnetism at T_N . Here, ZF- μ^+ SR is sensitive to weak local magnetic (dis)order in samples exhibiting quasistatic paramagnetic moments. The ZF- μ^+ SR spectrum, however, lacks any oscillatory signal even at 1.8 K, although the first minimum is observed around $0.01 \mu\text{s}$ (see Fig. 2). The spectra were hence fitted by a combination of two dynamic Gaussian Kubo-Toyabe (DGKT) signals and a fast- and slow-relaxing nonoscillatory signal (below T_N). One of the two DGKT signals appears only below T_N , while the other only above T_N . The former signal and the two nonoscillatory signals are thus due to the internal fluctuating fields and the latter due to the nuclear magnetic field of ^7Li and ^{55}Mn :

$$A_0 P_{\text{ZF}}(t) = A_{\text{KT1}} G^{\text{DGKT}}(t, \Delta_1, \nu_1) \exp(-\lambda_{\text{KT1}} t) \\ + A_{\text{KT2}} G^{\text{DGKT}}(t, \Delta_2, \nu_2) \exp(-\lambda_{\text{KT2}} t) \\ + A_{\text{fast}} \exp(-\lambda_{\text{fast}} t) + A_{\text{tail}} \exp(-\lambda_{\text{tail}} t), \quad (1)$$

where A_0 is the empirical maximum muon decay asymmetry, A_{KT1} , A_{KT2} , A_{fast} , and A_{tail} are the asymmetries associated with the four signals. λ_{KT1} , λ_{KT2} , λ_{fast} , and λ_{tail} are their relaxation rates, Δ_1 and Δ_2 are the static widths of the local frequencies at the disordered sites, and ν_1 and ν_2 are the field fluctuation rates. Here, $A_{\text{KT1}}=0$ above T_N , whereas $A_{\text{KT2}}=0$ below T_N . When $\nu=0$, $G^{\text{DGKT}}(t, \Delta, \nu)$ is the static Gaussian Kubo-Toyabe function $G_{\text{zz}}^{\text{KT}}(t, \Delta)$ given by

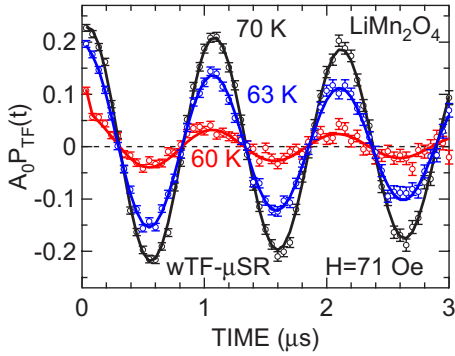


FIG. 3. (Color online) Weak transverse field (wTF)- μ^+ SR spectrum for LiMn_2O_4 obtained at 70, 63, and 60 K with $H = 71$ Oe at TRIUMF. Here, $A_0 P_{\text{TF}}(t) = A_{\text{TF}} \exp(-\lambda_{\text{TF}} t)^\beta \cos(\omega_\mu t + \phi) + A_{\text{fast}} \exp(-\lambda_{\text{fast}} t)$. The first term corresponds to the oscillation due to wTF, whereas the second term corresponds to the fast relaxation due to the disordered moments.

$$G_{zz}^{\text{KT}}(t, \Delta) = \frac{1}{3} + \frac{2}{3} (1 - \Delta^2 t^2) \exp\left(-\frac{\Delta^2 t^2}{2}\right). \quad (2)$$

Since the A_{fast} signal appears below T_N and in the vicinity of T_N , the A_{fast} signal is essentially the same as the A_{KT1} signal. This is because, in the fast-fluctuation limit ($\nu \gg \Delta$) in zero field, $G^{\text{DGKT}}(t, \Delta, \nu) \sim \exp(-\lambda t)$.¹⁷

The other three samples, i.e., LMO with $x=0.05, 0.1,$ and 0.15 , all clearly exhibit a KT-type relaxation at 1.8 K that is similar to the sample with $x=0$, as shown in Fig. 2. This suggests that LMO with $x>0$ undergoes a magnetic transition at low T ; and their magnetic structures are most likely identical to that for LiMn_2O_4 , although V_{Mn} increases with increasing x . It should be noted that the DGKT-type behavior due to randomly oriented magnetic moments is different from that of a typical dilute spin glass, for which the ZF spectrum is well explained by a Lorentzian KT function.^{18,19}

Figure 3 shows the weak transverse field (wTF)- μ^+ SR spectrum for LiMn_2O_4 obtained at $H=71$ Oe to demonstrate a drastic change at T_N . Here, “weak” means relative to the spontaneous internal fields (H_{int}) in the ordered state. A wTF- μ^+ SR technique is sensitive to local magnetic order via the shift of the μ^+ spin precession frequency and the enhanced μ^+ spin relaxation. As T decreases from 70 K, the oscillation amplitude due to a wTF decreases rapidly, indicating the appearance of H_{int} .

Figure 4 shows the T dependence of Δ_1 together with the normalized wTF asymmetry ($N_{A_{\text{TF}}}$), which roughly corresponds to the volume fraction of paramagnetic phases in the sample, and χ for the four LMO samples. The $N_{A_{\text{TF}}}(T)$ curve indicates that all the samples exhibit the magnetic transition with $T_N^{\text{mid}} \sim 61$ K for $x=0$, ~ 27 K for $x=0.05$, ~ 26 K for $x=0.1$, and ~ 23 K for $x=0.15$, where T_N^{mid} is defined as T at which $N_{A_{\text{TF}}} = 0.5$.

The $N_{A_{\text{TF}}}(T)$ curve is quite consistent with the $\chi(T)$ curve; that is, the $\chi(T)$ curve measured under ZFC mode starts to deviate from that measured in the FC mode below T_N , suggesting the development of a freezing component. Since $N_{A_{\text{TF}}} \sim 0$ below T_N , the four samples are assigned to be

$\sim 100\%$ magnetic below T_N . The results also indicate that T_N for the samples with $x>0$ is most likely the T_f of disordered moments. The substitution of Mn by Li decreases the amount of JT-active Mn^{3+} , stabilizes the cubic phase at low T ,¹² and annihilates charge ordering. As a result, a small amount of x (~ 0.05) is thought to reduce $T_N=61$ K drastically down to $T_f=27$ K, as reported for $(\text{Li}_x\text{Zn}_{1-x})\text{V}_2\text{O}_4$.²⁰

Figure 5 shows a tentative phase diagram of LMO using the present μ^+ SR and χ measurements together with previous χ data.¹³ Although the phase boundary between the AF and SG phases is still ambiguous at present, it is clearly understood that T_N is very sensitive to x . This is presumably the main reason for the discrepancy of T_N and the magnetic structure of LiMn_2O_4 in past reports.^{5–8} We wish to emphasize that the present μ^+ SR experiment confirms the existence of the magnetic transition for LMO with $x>0$, because, based only on the χ measurements, it is difficult to judge whether the origin of T_N and/or T_f is intrinsic.

As seen in Fig. 4(a), Δ_1 has a finite value below T_N or T_f , and, as T decreases, Δ_1 increases with decreasing slope; that is, an order-parameter-like behavior as expected for H_{int} . The four $\Delta_1(T)$ curves are very similar each other, although the magnitude of Δ_1 at 1.8 K decreases with increasing x , consistent with the fact that both the number of Mn ions and their effective magnetic moment (μ_{eff}) decreases with increasing x . In spite of the several neutron studies,^{6–8} the AF-ordered moment for LiMn_2O_4 is still unknown. Assuming that the ordered moment is comparable to $\mu_{\text{eff}} (=4.52\mu_B)$,⁵ and the μ^+ s experiencing H_{int} are bound to oxygen—the center of the four nearest neighboring Mn ions and 0.191 nm away from the Mn ions,⁴ a simple dipolar field calculation provides that the highest H_{int} is 32 kOe ($=600$ MHz) for a ferromagnetic arrangement. The magnitude of $\Delta_1(1.8$ K) ($\sim 200 \times 10^6 \text{ s}^{-1}$) is therefore reasonable for H_{int} due to Mn^{3+} and Mn^{4+} moments. It should be noted that, ν_1 at low T in LiMn_2O_4 are almost static on the μ^+ lifetime, as evidenced by our observation that $\nu_1 \leq 0.5 \times 10^6 \text{ s}^{-1}$ and $\lambda_{\text{KT1}} \leq 0.3 \times 10^6 \text{ s}^{-1}$ below 40 K, i.e., negligibly small compared with Δ_1 .

B. Jahn-Teller transition around 280 K

In order to elucidate the magnetic behavior near $T_{\text{JT}} = 280$ K, we have measured ZF and two LF- μ^+ SR spectra at each T point up to 320 K to determine Δ_2 and ν_2 precisely by a DGKT function [by the second and fourth terms in Eq. (1)] (see Fig. 6). This is because the change in the μ^+ SR parameters at T_{JT} is expected to be very small, as it is not magnetic in origin.

Figure 7 shows the T dependences of ν_2 , Δ_2 , and χ^{-1} for the four LMO samples. For the LiMn_2O_4 sample, as T increases from 50 K, ν_2 decreases monotonically up to 100 K, then increases with increasing the slope, finally reaches the maximum at ~ 270 K, and then decreases with further increasing T . The $\Delta_2(T)$ curve exhibits a sudden decrease at ~ 270 K accompanying the maximum in ν_2 . Since the $\chi(T)$ curve shows a small cusp at 275 K due to orbital ordering of Mn^{3+} at T_{JT} ,⁹ the peak of the $\nu_2(T)$ curve and the sudden decrease in Δ_2 are naturally assigned to be caused by the JT

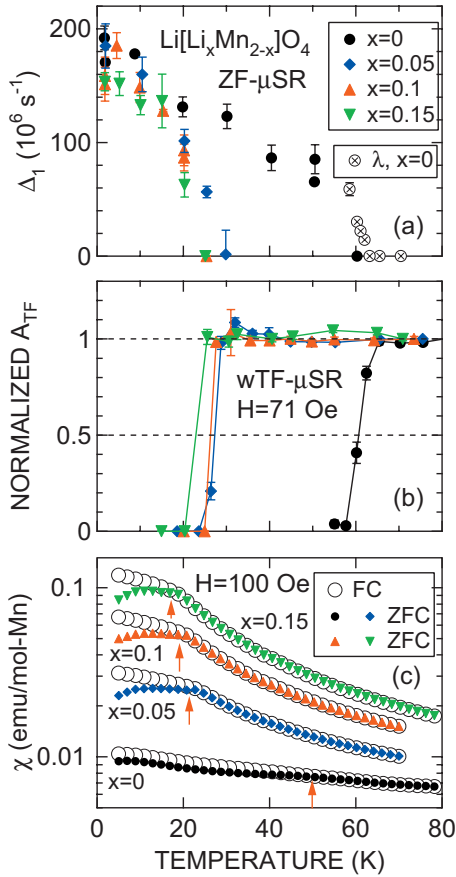


FIG. 4. (Color) T dependences of (a) the field distribution width Δ_1 , (b) the normalized wTF asymmetry [$N_{A_{\text{TF}}}=A_{\text{TF}}/A_{\text{TF}}(300 \text{ K})$], and (c) χ for LMO. χ was measured in both field-cooling (FC) and zero-field-cooling (ZFC) modes with $H=100 \text{ Oe}$. Crossed open circles in (a) show the $\lambda_{\text{fast}}(T)$ curve for LiMn_2O_4 , which continue to the $\Delta_1(T)$ curve with decreasing T . Red arrows in (c) show T_N determined by χ .

transition. During the JT transition, elastic softening was clearly observed.³ The maximum in the $\nu_2(T)$ curve is therefore most likely a consequence of a critical slowing down toward T_{JT} due to the spin-phonon interaction, as reported recently for DyVO_4 .²¹ Additionally, it is reasonable that Δ_2 in the high- T cubic phase is smaller than that in the low- T orthorhombic phase.

For the samples with $x=0.05-0.15$, although there are no anomalies in the $\chi^{-1}(T)$ curve, the $\nu_2(T)$ curve still exhibits a maximum at $\sim 270 \text{ K}$, and Δ_2 decreases with increasing T above $\sim 270 \text{ K}$, while both changes are suppressed with increasing x . The wTF- $\mu^+\text{SR}$ measurements clearly confirm the absence of any $x=0$ contaminant phase in the samples with $x \geq 0.05$ [see Fig. 4(b)]. More precisely, the $\Delta_2(T)$ curve below $\sim 320 \text{ K}$ shows that the transition occurs over a wider T range for the $x > 0$ sample. That is, as T decreases from 320 K , Δ_2 for the $x=0.05-0.15$ samples starts to increase below 290 K with decreasing slope, and seems to level off to its maximum value below $\sim 200 \text{ K}$ —i.e., the transition width (δT_{JT}) is $\sim 90 \text{ K}$, whereas $\delta T_{\text{JT}} \sim 30 \text{ K}$ for LiMn_2O_4 (see Fig. 8).

Therefore, $\mu^+\text{SR}$ detects the appearance of a short-range cooperative JT distortion ($T_{\text{SRJT}}^{\text{on}}$) even in the samples with

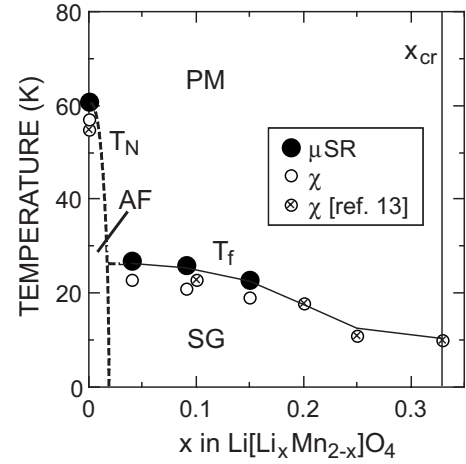


FIG. 5. Magnetic phases in $\text{Li}[\text{Li}_x\text{Mn}_{2-x}\text{O}_4]$. T_N indicates an antiferromagnetic (AF) transition temperature, T_f a spin-freezing temperature, $x_{\text{cr}}=1/3$ the solubility limit of Li, PM a paramagnetic phase, and SG a spin-glass-like phase. Although the phase boundary between the AF and SG phases (broken lines) is not clear at present, T_N is found to decrease rapidly with increasing x .

$x=0.15$ at $\sim 280 \text{ K}$, whereas no anomalies are detected by χ and other macroscopic measurements for LMO with $x \geq 0.05$. As T decreases from $T_{\text{SRJT}}^{\text{on}}$, the short-range cooperative JT distortion develops down to the end point of T_{JT} ($T_{\text{SRJT}}^{\text{end}}=T_{\text{SRJT}}^{\text{on}}-\delta T_{\text{JT}}$). It is thus found that $T_{\text{SRJT}}^{\text{on}}$ is unchanging with x but the change in physical properties at $T_{\text{SRJT}}^{\text{on}}$ reduces with x and eventually disappears for LMO with $x \geq 0.05$. We note that a very similar $\Delta_2(T)$ curve measured in the T range up to 380 K (far above T_{JT}) was reported for LMO with $x=0.04$ in Ref. 14 and for $x=0$ in Ref. 15; in the latter, the maximum in the $\nu_2(T)$ curve was also seen. Both authors however explained the change in the $\Delta_2(T)$ curve at $\sim 280 \text{ K}$ not by the cooperative JT distortion but by Li^+ diffusion.

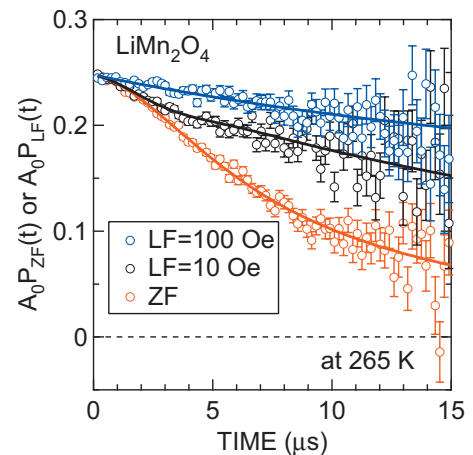


FIG. 6. (Color) ZF and LF- $\mu^+\text{SR}$ spectra for LiMn_2O_4 at 265 K obtained at ISIS. The solid lines represent the global fitting result using the second and fourth terms of Eq. (1). A slowly exponential relaxation signal ($\lambda_{\text{tail}} \sim 0$) comes from the muons stopped outside the sample, mainly in the silver holder. Since $A_{\text{tail}}/A_{\text{KT2}} \sim 0.03/0.21$ in the whole T range measured, 88% of the muons stop in the sample while the remainder stop in the silver.

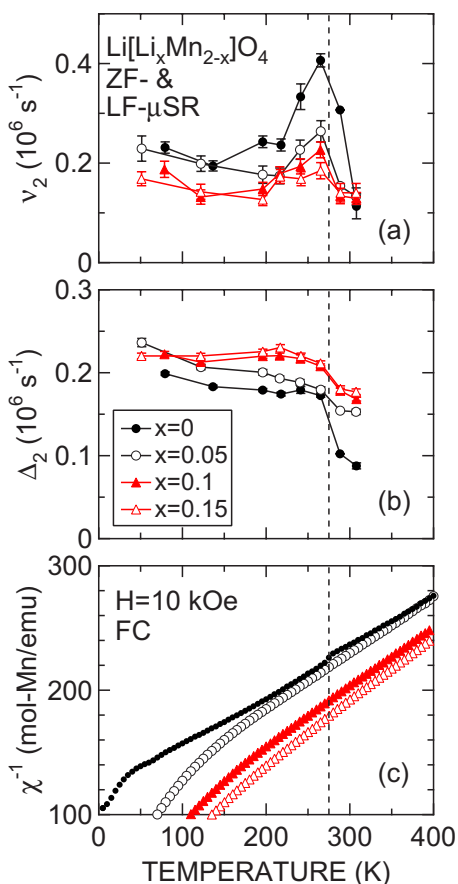


FIG. 7. (Color online) T dependences of (a) the field fluctuation rate (ν_2), (b) the field distribution width (Δ_2), and (c) $1/\chi$ for LMO with $x=0, 0.05, 0.1$, and 0.15 . The data were obtained by fitting the ZF and LF- μ^+ SR spectrum (see Fig. 6) using Eq. (1). The spectra were measured in at Riken-RAL of ISIS in the time domain up to $20 \mu\text{s}$. χ was measured in FC mode with $H=10 \text{ kOe}$. λ_{KT2} ranges from 0.02×10^6 to $0.05 \times 10^6 \text{ s}^{-1}$ and is almost T independent above 100 K.

The present result is also consistent with that of the recent elastic–anelastic measurements on LMO with $x \leq 0.08$.¹¹ The structural transition temperature determined by the T dependence of Young's modulus (T_{JT}^E) was reported to decrease from 280 to 240 K with increasing x from 0 to 0.02, and then T_{JT}^E was almost x independent ($\sim 210 \text{ K}$) for LMO with $x=0.04-0.08$. Since $T_{SRJT}^{\text{end}} \sim 200 \text{ K}$ for the $x=0.05-0.15$ samples, the macroscopic elastic anomaly is found to be detected at T_{SRJT}^{end} . This is thought to be very reasonable, since the long-range order detectable by macroscopic measure-

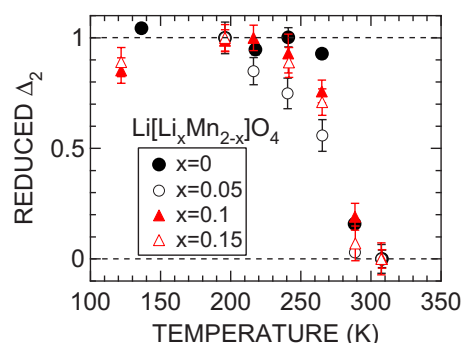


FIG. 8. (Color online) T dependences of the reduced Δ_2 of Fig. 7(b) for LMO with $x=0, 0.05, 0.1$, and 0.15 .

ments often appears below the temperature at which the development of short-range order is completed, as in the case for several cobalt oxides.^{23,24}

IV. CONCLUSION

The present result impacts research on rechargeable lithium batteries. In order to improve the performance of such batteries, the cubic phase is stabilized by substitution of Mn with other elements.^{1,22} The effects of such substitution on the lattice stability are usually examined by XRD and/or DSC measurements. However, the fact that μ^+ SR is able to provide information on the appearance of the short-range cooperative JT distortion, the only technique to our knowledge that is able to do so, suggests that substitution effects in LMO should be reexamined by combining μ^+ SR and electrochemical analyses. Furthermore, such studies should probably be carried out not only for LMO, but also for related battery materials such as LiCoO_2 and LiNiO_2 .

ACKNOWLEDGMENTS

This work was performed both at the RIKEN-RAL Muon Facility at the ISIS and TRIUMF. We thank the staff of ISIS and TRIUMF for help with the μ^+ SR experiments. We also appreciate Y. Motome and M. Udagawa of the University of Tokyo for discussion. Furthermore, we thank Y. Kondo of TCRDL for ICP-AES analysis and H. Wakabayashi of OCU for sample preparation and electrochemical characterization. J.S. and Y.I. are supported by the KEK-MSL Inter-University Program for Oversea Muon Facilities. J.H.B. is supported at UBC by CIAR, NSERC of Canada, and at TRIUMF by NRC of Canada. K.H.C. is supported by NSERC of Canada.

*Electronic address: e0589@mosk.tytlabs.co.jp

¹G. Amatucci and J.-M. Tarascon, *J. Electrochem. Soc.* **149**, K31 (2002), and references cited therein.

²A. Yamada and M. Tanaka, *Mater. Res. Bull.* **30**, 715 (1995).

³J. Sugiyama, T. Tamura, and H. Yamauchi, *J. Phys.: Condens. Matter* **7**, 9755 (1995).

⁴H. Yamaguchi, A. Yamada, and H. Uwe, *Phys. Rev. B* **58**, 8 (1998).

⁵J. Sugiyama, T. Hioki, S. Noda, and M. Kontani, *J. Phys. Soc. Jpn.* **66**, 1187 (1997).

⁶Y. Oohara, J. Sugiyama, and M. Kontani, *J. Phys. Soc. Jpn.* **68**, 242 (1999).

- ⁷I. Tomeno, Y. Kasuya, and Y. Tsunoda, *Phys. Rev. B* **64**, 094422 (2001).
- ⁸J. E. Greedan, C. R. Wiebe, A. S. Wills, and J. R. Stewart, *Phys. Rev. B* **65**, 184424 (2002).
- ⁹J. Rodriguez-Carvajal, G. Rousse, C. Masquelier, and M. Hervieu, *Phys. Rev. Lett.* **81**, 4660 (1998).
- ¹⁰A. Yamada, *J. Solid State Chem.* **122**, 160 (1996).
- ¹¹A. Paolone, R. Cantelli, B. Scrosati, P. Reale, M. Ferretti, and C. Masquelier, *Electrochem. Commun.* **8**, 113 (2006).
- ¹²H. G. Schimmel, W. Montfrooij, G. J. Kearley, V. W. J. Verhoeven, and I. M. deSchepper, *Phys. Rev. B* **63**, 214409 (2001).
- ¹³P. Endres, B. Fuchs, S. Kemmler-Sack, K. Brandt, G. Faust-Becker, and H.-W. Praas, *Solid State Ionics* **89**, 221 (1996).
- ¹⁴C. T. Kaiser, V. W. J. Verhoeven, P. C. M. Gubbens, F. M. Mulder, I. de Schepper, A. Yaouanc, P. Dalmas de Réotier, S. P. Cottrell, E. M. Kelder, and J. Schoonman, *Phys. Rev. B* **62**, R9236 (2000).
- ¹⁵M. J. Ariza, D. J. Jones, J. Rozière, J. S. Lord, and D. Ravot, *J. Phys. Chem. B* **107**, 6003 (2003).
- ¹⁶T. Ohzuku, S. Kitano, M. Iwanaga, H. Matsuno, and A. Ueda, *J. Power Sources* **68**, 646 (1997).
- ¹⁷G. M. Kalvius, D. R. Noakes, and O. Hartmann, in *Handbook on the Physics and Chemistry of Rare Earths*, edited by K. A. Gschneidner Jr., L. Eyring, and G. H. Lander (North-Holland, Amsterdam, 2001), Vol. 32, Chap. 206.
- ¹⁸Y. J. Uemura, T. Yamazaki, R. S. Hayano, R. Nakai, and C. Y. Huang, *Phys. Rev. Lett.* **45**, 583 (1980).
- ¹⁹Y. J. Uemura, T. Yamazaki, D. R. Harshman, M. Senba, and E. J. Ansaldo, *Phys. Rev. B* **31**, 546 (1985).
- ²⁰Y. Ueda, N. Fujiwara, and H. Yasuoka, *J. Phys. Soc. Jpn.* **66**, 778 (1997).
- ²¹S. J. Blundell, I. M. Marshall, W. Hayes, and F. L. Pratt, *Phys. Rev. B* **70**, 212408 (2004).
- ²²K. Ariyoshi, E. Iwata, M. Kuniyoshi, H. Wakabayashi, and T. Ohzuku, *Electrochem. Solid-State Lett.* **9**, A557 (2006).
- ²³J. Sugiyama, J. H. Brewer, E. J. Ansaldo, H. Itahara, K. Dohmae, Y. Seno, C. Xia, and T. Tani, *Phys. Rev. B* **68**, 134423 (2003).
- ²⁴J. Sugiyama, H. Nozaki, J. H. Brewer, E. J. Ansaldo, T. Takami, H. Ikuta, and U. Mizutani, *Phys. Rev. B* **72**, 064418 (2005).